Langmuir

ARTICLE

pubs.acs.org/Langmuir

Zipper and Layer-by-Layer Assemblies of Artificial Photosystems Analyzed by Combining Optical and Piezoelectric Surface Techniques

Mariya Porus,[†] Plinio Maroni,[†] Rajesh Bhosale,[‡,§] Naomi Sakai,[‡] Stefan Matile,[‡] and Michal Borkovec*[,†]

[†]Department of Inorganic, Analytical, and Applied Chemistry and [‡]Department of Organic Chemistry, University of Geneva, Geneva, Switzerland

[§]Department of Chemistry, Massachusetts Institute of Technology, Cambridge, Massachusetts 02139, United States

ABSTRACT: Quartz crystal microbalance (QCM) and surface plasmon resonance (SPR) were used to study zipper and layer-by-layer multilayer assemblies of artificial photosystems based on naphthalenediimides (NDIs) attached to an oligophenylethynyl (OPE-NDI) or *p*-oligophenyl (POP-NDI) backbone in dry and wet state. For the most interesting OPE-NDI zipper, one obtains for the dry film a monolayer thickness of 1.85 nm and a density of 1.58 g/cm^3, while the wet film has a larger monolayer thickness of 3.6 nm with a water content of 36%. The dry thickness of a monolayer in OPE-NDI zippers corresponds to about one-half of the length of the OPE scaffold in agreement with the proposed structure of the zipper. The low water content of the OPE-NDI films confirms their compact structure. The dry monolayer thickness of the POP-NDI films of 1.45 nm is smaller than that for the OPE-NDI films, which is probably related to a tilt of the POP scaffolds within the adsorbed layer. The POP-NDI films swell in water much more substantially, suggesting a much more open structure. These features are in excellent agreement with the better photophysical performance of the OPE-NDI assemblies when compared to the POP-NDI films.

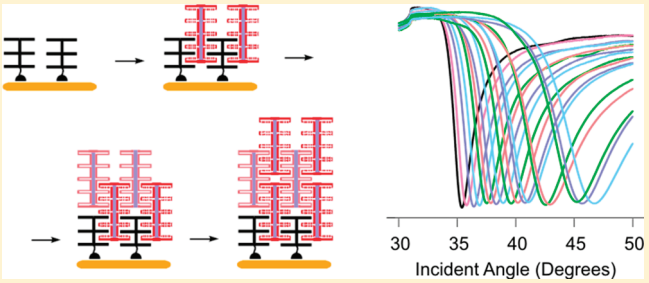

INTRODUCTION

The construction of ordered and oriented multicomponent architectures is an important topic in current research on supramolecular functional systems.[1−41] One of the best-established methods toward this objective is layer-by-layer (LBL) assembly.[25−33] In this approach, a negatively (or positively) charged monolayer is prepared first. This study uses a monolayer of lipoic acid **1** on gold, that is, Au-**1** (Figure 1). The anionic Au-**1** is dipped into a solution of polycationic (or polyanionic) oligomers or polymers. One example used in this study is the cationic oligomers **2** that are composed of red naphthalenediimides (NDIs) attached along an oligophenylethynyl (OPE) scaffold.[34] The obtained formal bilayer Au-**1**-**2** is then washed to remove weakly adsorbed oligomers. Dipping of the overall cationic Au-**1**-**2** into a solution of the complementary anionic propagators such as OPE-NDI hybrid **3** gives the anionic Au-**1**-**2**-**3**, which in turn is incubated with cationic propagator **2** to give Au-**1**-**2**-**3**-**2**, and so on.

To improve the "fuzzy" organization of LBL architectures,[25] the zipper assembly has been introduced.[34−41] In this approach, the assembly process begins with initiators such as **4** in place of lipoic acid **1** used for LBL assembly. Initiator **4** is equipped with anionic NDI acceptors along an OPE scaffold half as long as in propagators **2** and **3**, and a disulfide tail for covalent immobilization on gold (Figure 1). Incubation of Au-**4** monolayers with cationic OPE-NDI propagators **2** is expected to give Au-**4**-**2** bilayers, where the lower half of the cationic NDIs of **2** interdigitates with the anionic ones of the initiator **2** to form a π-stack. The upper half of the cationic NDIs of **2** remains free as "sticky end" on the surface of Au-**4**-**2** to zip up with the lower half of the anionic propagator **3**, which leaves sticky ends on Au-**4**-**2**-**3** to zip up with the lower half of propagator **2**, and so on. The resulting OPE-NDI zipper architectures Au-**4**-(**2**-**3**-)$_n$ are composed of interdigitating layers with intra- and interlayer recognition sites. As a result, face-to-face π-stacks should end up aligned along strings of rigid-rod scaffolds. This architecture is of interest to build e^- transporting pathways, here the NDI stacks, along strings of h^+ transporting channels, here the OPE rods. The coaxial alignment of e^- and h^+ channels on the molecular level is of interest in optoelectronics to combine high charge mobility with large donor−acceptor interfaces. This architecture is referred to as supramolecular n/p-heterojunction (SHJ).[1]

Zipper assembly has been studied for various NDIs of different color and redox properties, and with *p*-oligophenyl (POP) scaffolds in place of the OPEs, that is, Au-**5**-(**6**-**7**-)$_n$ (Figure 2).[35,38,40] Moreover, the different systems could be combined to build SHJ photosystems with oriented antiparallel redox gradients (i.e., OMARG-SHJs).[39] Different from the 10 NDIs along the OPE scaffold in **2** and **3**, POP-NDI hybrids **6** and **7** contain only 8 NDIs along a shape-persistent scaffold of similar length. Whereas the repeat distance in the OPE scaffold roughly matches the repeat distance of NDI-stacks formed by zipper assembly, the repeat distance in the POP scaffold is thus slightly too long (0.5 vs 0.34 nm). As a result, the

Received: March 1, 2011
Revised: April 8, 2011
Published: April 28, 2011

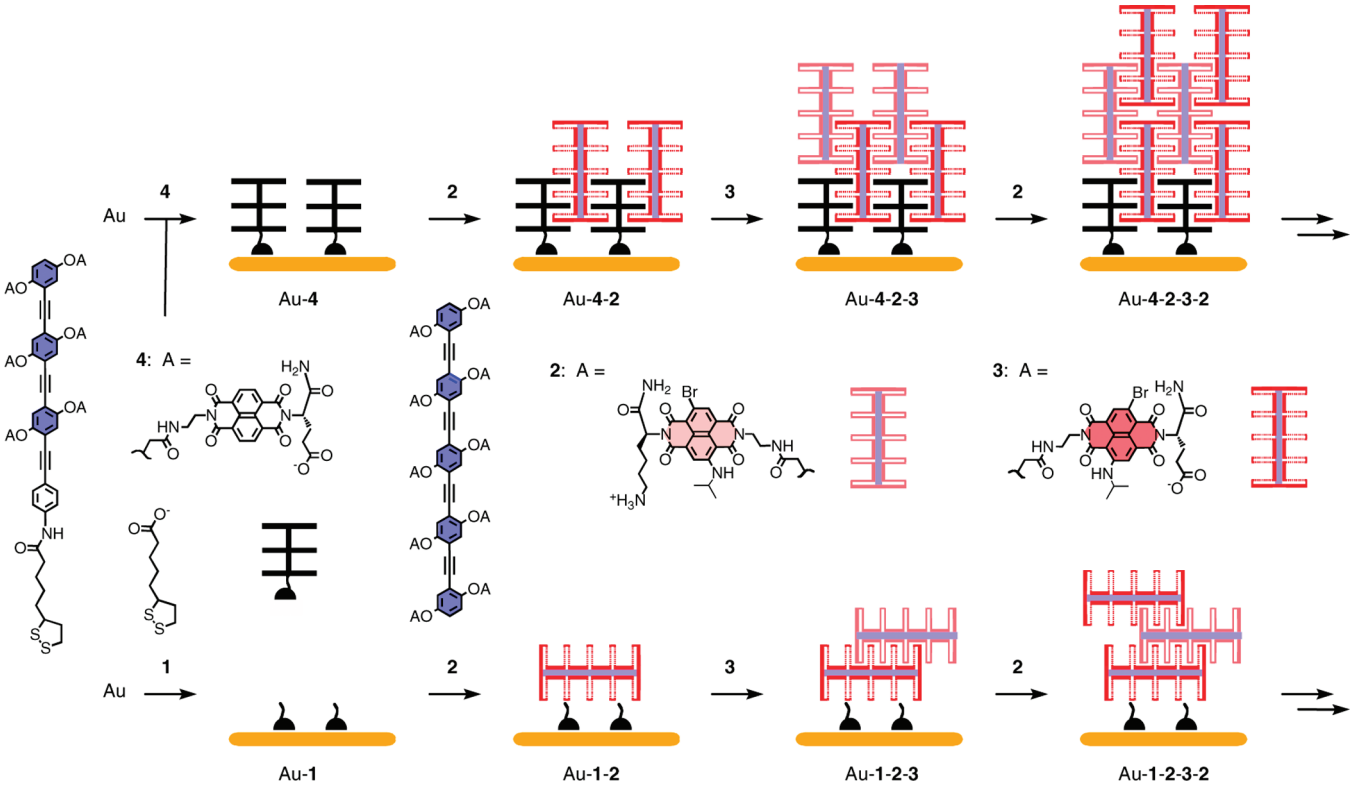

Figure 1. Pictorial representation of the zipper assembly (top) and LBL assembly (bottom) of OPE-NDI architectures with full structure of all building blocks. The suprastructures are speculative representations and drawn with the only intention to clarify the described concepts.

POP scaffold in zipper assembly Au-**5**-(**6**-**7**-)$_n$ should twist into a more helical architecture to allow for intact $\pi-\pi$ interactions in the NDI stacks (Figure 2). This topological mismatch in POP-NDI zippers Au-**5**-(**6**-**7**-)$_n$ has been shown to reduce the activity compared to the topologically matching OPE-NDI zippers Au-**4**-(**2**-**3**-)$_n$.[35]

In general, structure and function of zipper architectures were better those that of LBL architectures, and OPE architectures were better than POP architectures.[35,38,40,41] Zipper architectures generate more photocurrent and have better critical thickness. The critical thickness, referring to the number of layers where the onset of photocurrent saturation by charge recombination occurs, is an established measure for the importance of supramolecular organization for function. The much slower kinetics of zipper compared to LBL assembly supports the occurrence of self-repair. A critical piece of evidence in support of their difference is that operational zipper assembly can be inhibited by capping with short *p*-quaterphenyl terminators similar to initiator **4**, whereas LBL assembly is insensitive to capping.[35] These capping controls are important because they demonstrate that zipper assembly operates with interdigitating sticky ends, whereas LBL does not. Both zipper and LBL architectures can be assembled at low micromolar concentrations and show neither disassembly nor bleaching during routine use for photocurrent generation without special precautions (e.g., oxygen removal). These interesting results called for more detailed characterization of the resulting surface layers. Here, we report on combined SPR and QCM-D studies of matched and mismatched zipper assemblies Au-**4**-(**2**-**3**-)$_n$ and Au-**5**-(**6**-**7**-)$_n$, respectively, in comparison to the corresponding LBL architectures Au-**1**-(**2**-**3**-)$_n$ and Au-**1**-(**5**-**6**-)$_n$.

EXPERIMENTAL SECTION

Materials. OPE-NDI hybrids **2**−**4** were prepared by multistep organic synthesis following previously reported procedures.[35] The spectroscopic and analytical data of the final products were identical with previously reported ones, confirming the structure and the purity of the compounds.

The substrates for the SPR experiments were prepared as follows. BK7 glass slides of dimensions 10 × 10 × 1 mm^3 (Glasstechnology, Switzerland) were cleaned in a mixture of water, hydrogen peroxide (35%), and ammonia (25%) at a volume ratio of 5:1:1 at 80 °C for 15 min. The cleaned slides were coated by vapor deposition with a chromium adhesive layer with a thickness not exceeding 1−1.5 nm and subsequently with a gold film of thickness within 43−46 nm under high vacuum (5 × 10^{-7} mbar) with a deposition rate of 1 nm/s. SF10 glass slides coated with a gold layer of 40 nm in thickness were purchased from Phasis (Geneva, Switzerland). Prior to use, the slides were washed in 2% aqueous Helmanex solution, rinsed extensively with pure water, and treated in a UV−O cleaner during 20 min.

Gold coated quartz crystals (Q-Sense, Gotheborg, Sweden) were used as substrates for the QCM experiments and were cleaned by ultrasonication in 2% aqueous Helmanex solution during 15 min followed by cleaning in an air plasma (Harrick, USA) for 4 min.

Multilayer Preparation. Solutions were prepared as described earlier.[35] Namely, **2** and **3** in a buffer solution containing a 0.25 mM phosphate buffer of pH 7 and 0.5 M NaCl in 50% aqueous 2,2,2-trifluoroethanol (TFE), and **6** and **7** in a 0.5 mM phosphate buffer (pH 7) and 0.1 M NaCl in 50% aqueous TFE. The LBL assemblies were initiated in a 10 mM solution of **1** in 0.25 mM sodium phosphate buffer at pH 7 and 0.25 M NaCl in 50% aqueous TFE, while the zipper assemblies were initiated in a 0.3 mM solution of **4** in a mixture of dimethylformamide and water at a ratio of 5:1 overnight. The wafers

dx.doi.org/10.1021/la2007815 |*Langmuir* 2011, 27, 7213–7221

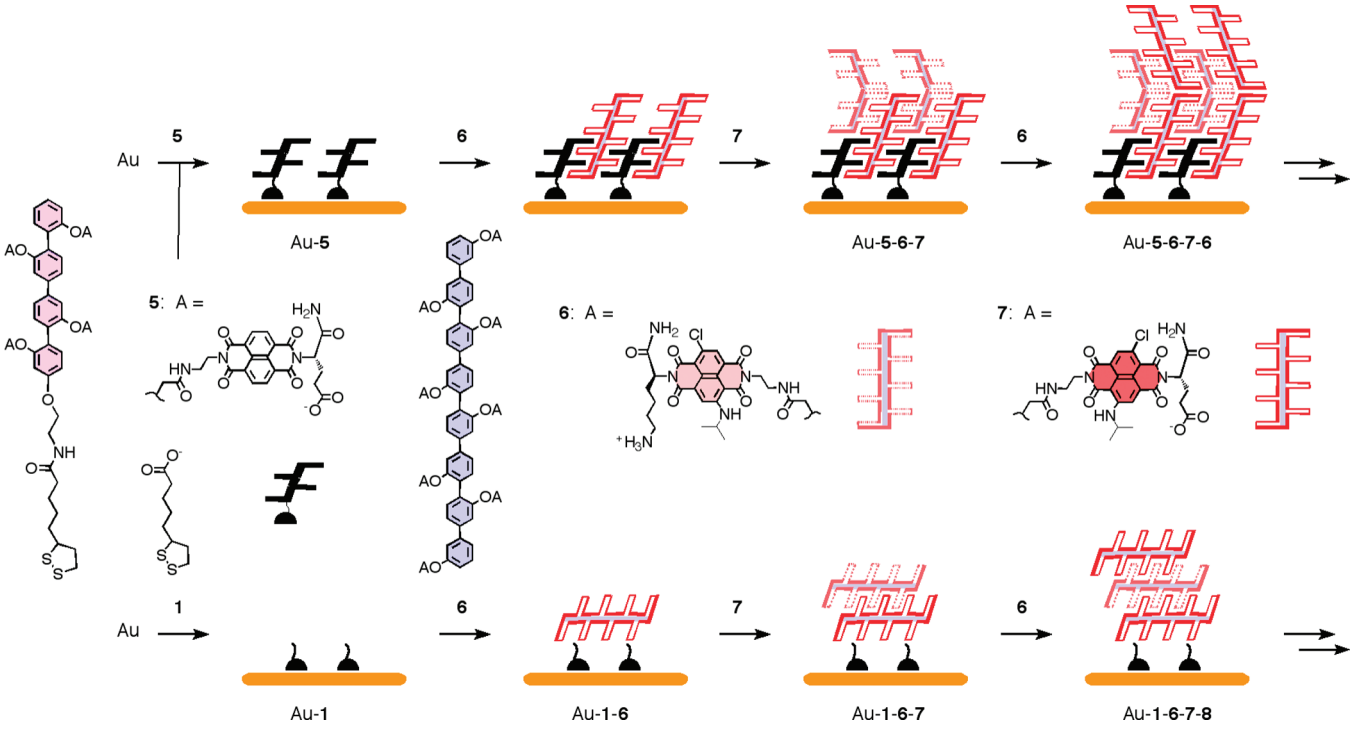

Figure 2. Pictorial representation of zipper assembly (top) and LBL assembly (bottom) of POP-NDI architectures. Topological rod-stack mismatch in these systems is expected to result in slightly disorganized, helically twisted surface architectures. The suprastructures are speculative representations and drawn with the only intention to clarify the described concepts.

were rinsed afterward in the buffer solution for several minutes and subsequently in Milli-Q water. They were dried with nitrogen and incubated in solution **2** of concentration of 10 μM overnight. After the same rinsing procedure, a second layer of **3** was deposited from a concentration of 10 μM. Dipping the wafers in the solutions of positively and negatively charged compounds was repeated until the desired number of monolayers in the OPE-NDI LBL Au-**1**-(**2**-**3**-)$_n$ or zipper Au-**4**-(**2**-**3**-)$_n$ assembly was reached. For SPR measurements, the layers were adsorbed on glass slides, and for QCM measurements on QCM sensor plates. The same procedure was used for POP-NDI LBL Au-**1**-(**6**-**7**-)$_n$ and zipper Au-**5**-(**6**-**7**-)$_n$ assemblies whereby **1** and **5** (1 mM in 0.5 mM sodium phosphate, 0.5 M NaCl, 50% aqueous TFE buffer pH 7) were used as initiators.

Quartz Crystal Microbalance (QCM). The experiments were carried with a Q-Sense E4 (Gotheborg, Sweden) instrument in a flow through cell. This device uses the mechanical resonance of a quartz single crystal to detect the change in mass due to the formation of an adsorbed layer. As quartz is a piezoelectric material, it undergoes mechanical deformations in electric fields. By applying an alternating voltage, the crystal can be brought to oscillate at its resonance frequency. The change in the resonance frequency Δf is directly proportional to the adsorbed mass and is described by Sauerbrey equation[42]

$$\Delta f = -\frac{m}{C}\Gamma \qquad (1)$$

where m is the overtone number and $C = 0.0177\ \mu g\ Hz^{-1}\ cm^{-2}$ is the mass sensitivity constant.[43] The crystal with adsorbed film was installed in the cell. After the cell was filled with buffer solution, its resonance frequency was measured. The procedure was repeated after each incubation step.

Surface Plasmon Resonance (SPR). The experiments in dry state and in solution were carried out with an Optrel multiscope instrument (Berlin, Germany). The Kretschman's configuration cell is mounted horizontally in the common axis of the two goniometer arms. One arm carries a He−Ne laser of wavelength of 633 nm to obtain the plasmon excitation of the gold layer deposited on glass slide. A photodiode on the other arm is used to measure the intensity of the reflected light. The slide was mounted with a refractive-index matching fluid (Cargille Laboratories Inc., USA) on the base of an equilateral dispersing prism. To carry out SPR measurement in air, glass slides and prism made of BK7 glass (Optarius, U.K.) with a refractive index of 1.515 were used. In this configuration, the resonance angle was between 35° and 50°. For measurements in solution, the SF10 glass with a refractive index of 1.728 was used for slides and prism (Thorlabs, Germany). The prism−slide assembly was mounted on a Teflon flow-through cell and sealed with a rubber O-ring. For the fluid cell, the resonance angle lies in the range 50−65°. Regular glass cannot be used for the measurements with the fluid cell, as the SPR does not occur in the accessible angular range. The angular dependence of the SPR reflectivity was interpreted quantitatively with the two-slab model within the Abeles matrix formalism (Figure 4).[44,45] Once these parameters were obtained for the wafer, the properties of the adsorbed layer were determined with a three-slab model whereby the refractive index of the layer as well as its thickness were used as fitting parameters.

Scanning angle ellipsometry was also used to obtain the optical properties of these films. For the thicker films, the results were in good agreement with the SPR data. However, the ellipsometric technique is about 10 times less sensitive, and thus the properties of the thinner films remained inaccessible with ellipsometry.

Combined Data Analysis. The adsorbed mass Γ of the wet film as measured by QCM can be related to its thickness L as

$$\Gamma = \rho L \qquad (2)$$

where ρ is the wet density of the film. When the film is dry, the adsorbed mass Γ_h can be related similarly to its thickness L_h as

$$\Gamma_h = \rho_h L_h \qquad (3)$$

dx.doi.org/10.1021/la2007815 |*Langmuir* 2011, 27, 7213–7221

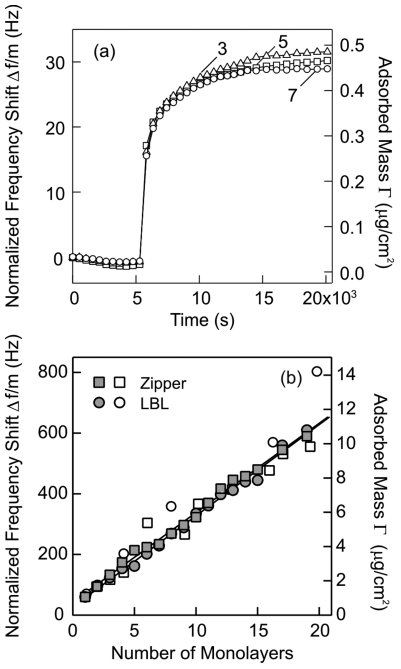

Figure 3. Analysis of OPE-NDI LBL film Au-**1**-(**2**-**3**-)$_n$ by QCM. (a) Frequency shift normalized to the overtone order as a function of time during the formation of the ninth layer. (b) Normalized frequency shift and wet mass as a function of the number of monolayers deposited for LBL and zipper assemblies (gray symbols). The open symbols correspond to the results for OPE LBL and zipper assemblies reported in ref 35.

where ρ_h is the dry density of the hybrid. The density of the wet film can be related to dry density by assuming an ideal mixing law as

$$\rho = \rho_s\phi + \rho_h(1-\phi) \quad (4)$$

where ϕ is the volume fraction of water and ρ_s = 1.186 g/cm^3 is the density of the buffer solution used at room temperature. Taking the ratio between eqs 2 and 3, one obtains

$$\phi = 1 - \frac{L_h}{L} \quad (5)$$

This relation can be used to estimate the water content of the film when the dry and wet thickness has been found from SPR measurements. Another way to obtain the water content is by comparing the refractive indices n and n_h in the wet and dry state, and by making use of the ideal mixing law

$$n = n_s\phi + n_h(1-\phi) \quad (6)$$

where n_s = 1.312 is the refractive index of the buffer solution. When the refractive indices are known, the refractive index increment can be obtained from the relation

$$\frac{dn}{dc} = \frac{n_h - n_s}{\rho_h} \quad (7)$$

RESULTS AND DISCUSSION

QCM and SPR have been used to characterize OPE-NDI surface assemblies obtained with the LBL Au-**1**-(**2**-**3**-)$_n$ and zipper Au-**4**-(**2**-**3**-)$_n$ techniques on gold surfaces in dry state and in aqueous solution. By combining these techniques, it is not only possible to obtain the adsorbed mass, thickness, and water content of these multilayers, but also permits to find additional physical properties of OPE-NDIs, such as their density or refractive index. These results are further compared with POP-NDI film assemblies obtained by LBL Au-**1**-(**6**-**7**-)$_n$ and zipper Au-**5**-(**6**-**7**-)$_n$ techniques.

Table 1. Properties of OPE-NDI Films as Directly Obtained from QCM and SPR Measurements

technique	quantity	LBL	zipper
QCM	adsorbed wet mass, Γ (μg/cm^2)	0.53 ± 0.02	0.52 ± 0.01
SPR, dry film	real part refractive index, n_h	1.48 ± 0.01	1.47 ± 0.01
	imaginary part refractive index, k_h	0.011 ± 0.006	0.012 ± 0.005
	layer thickness, L_h (nm)	1.94 ± 0.02	1.85 ± 0.05
SPR, wet film	real part refractive index, n	1.44 ± 0.01	1.43 ± 0.01
	imaginary part refractive index, k	0.002 ± 0.001	0.003 ± 0.004
	layer thickness, L (nm)	3.7 ± 0.1	3.6 ± 0.1

OPE-NDIs Films Probed by QCM. The formation of the multilayer can be followed by QCM as illustrated in Figure 3. One observes that the film attains its final state only after several hours. The different overtones lead to very similar frequency shifts as can be seen in Figure 3a. This correspondence suggests that the layer is rigid and compact. The corresponding negative frequency shifts as a function of the number of adsorbed monolayers are shown in Figure 3b. These results agree well with previously published QCM data on OPE-NDI layers.[35] The frequency shifts can be converted to adsorbed mass per unit area with eq 1, and the corresponding numbers are also shown in Figure 3b. Since the trapped solvent oscillates together with the adsorbed layer, this technique yields the wet mass of the film per unit area Γ including the trapped solvent. The adsorbed mass increases linearly with the increasing number of adsorbed monolayers. The slope of the best fit line yields a mass 0.53 ± 0.02 μg/cm^2 for the LBL assembly and 0.52 ± 0.01 μg/cm^2 for the zipper. These parameters are also summarized in Table 1. The nonzero intercept indicates that additional material adsorbed during the formation of the first few layers.

OPE-NDIs Probed by SPR. The reflected intensity of the bare gold layer in air is shown in Figure 4. To promote the adhesion of the subsequent gold layer, the glass slide was first coated with a thin chromium layer. The reflected intensity was therefore fitted with a two-slab optical model where the known refractive indices of 3.129 + 3.312i for chromium and 0.185 + 3.475i for gold were used.[46,47] Least squares fit yields a thickness of 0.82 ± 0.01 nm for the chromium layer and 43.4 ± 0.1 nm for the gold layer. Similar values were found for other metal coatings. The properties of the dry layer were determined by fitting the refractive index and the thickness in a three-slab model whereby the properties of the underlying gold and chromium slabs were kept fixed. A typical fit for such a dried LBL film is also shown in Figure 4. In this particular case, one obtains a refractive index of 1.284 + 0.009i and a thickness of 26 nm. For thin films, these parameters are strongly correlated and subject to errors. For thicker films, these parameters can be obtained reliably as will be discussed below.

The SPR reflection curves were measured for the progressive sequence of adsorbed multilayers, and the result is shown in Figure 5a. One observes that the reflection minimum shifts toward larger angles as the number of adsorbed monolayers

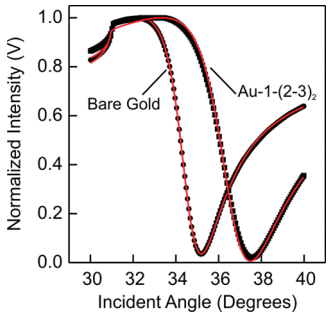

Figure 4. Comparison of experimental and fitted SPR reflectivity curves for the bare gold surface and a surface covered with OPE-NDI LBL assembly Au-**1**-(**2**-**3**)$_2$ in dry state.

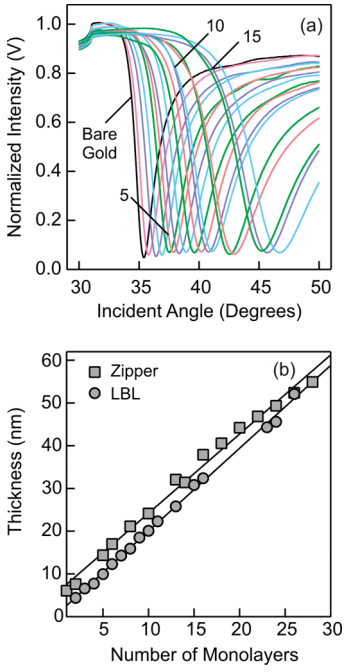

Figure 5. Analysis of dry OPE-NDI LBL film Au-**1**-(**2**-**3**-)$_n$ by SPR. (a) Series of SPR curves for different number of monolayers deposited within the LBL multilayer on gold-coated BK7 prism. (b) Thickness calculated from SPR as a function of the number of monolayers deposited for OPE-NDI assemblies obtained by LBL and zipper techniques.

increases. By fitting the reflection curve with the three-slab model, the refractive index and the layer thickness can be extracted. Figure 6 shows the real part of the refractive index and the slab thickness as a function of the number of adsorbed monolayers. One observes that the refractive index and the thickness can be both reliably determined only for larger number of monolayers. For a number of monolayers below about 20, these two parameters cannot be determined simultaneously due to correlations and are subject to large errors. Therefore, the refractive index was extracted for the thickest layers, and the best value found for the OPE-NDI layer was 1.48 ± 0.01 for the real part and 0.011 ± 0.002 for the imaginary part. These values for the LBL assembly are also summarized in Table 1 and compared with the very similar values for the zipper assembly. Clearly, no differences between the refractive indices of the LBL and zipper

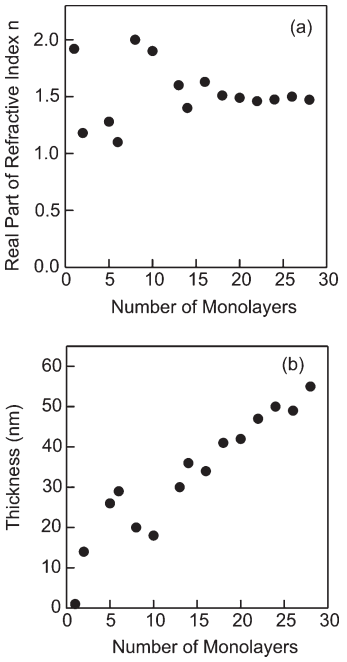

Figure 6. Analysis of dry OPE-NDI zipper film Au-**4**-(**2**-**3**)$_n$ by SPR. Fitted values of (a) real part of refractive index and (b) corresponding thickness of the adsorbed layer as a function of the number of monolayers deposited.

assemblies are expected. By fixing these refractive indices in least-squares fit of the SPR curves, the layer thickness could now be determined reliably even for thinner layers. The results are presented in Figure 5b. One observes a linear increase in the layer thickness with increasing number of monolayers adsorbed. A linear fit gives a thickness of a single layer of 1.94 ± 0.02 nm for the LBL assembly and 1.85 ± 0.05 nm for the zipper assembly. The larger intercept for the zipper assembly is probably related to the initiator **4** used. The observed monolayer thickness is somewhat larger but still comparable to the thickness of 1.5 nm reported for the zipper assembly by atomic force microscopy (AFM) measurements in dry state.[35] The discrepancy could be related to surface roughness, which will contribute to the thickness in the optical measurements but not to the AFM imaging of a single step. Approximately matching with the half the length of the OPE scaffold, the slightly reduced thickness of OPE-NDI zipper compared to LBL assembly could reflect their better, more compact organization.

Similar SPR measurements were carried out in the buffer solution. Since the intensity minimum of the reflected light is inaccessible for the normal glass prism, a prism made of glass with a higher refractive index was used. With that prism, the minimum of the bare gold interface was situated at about 53° in solution. The layer thickness and the refractive indices for gold were also determined with a two-slab model in water and the values were in good agreement with those obtained in air. During the successive formation of the multilayers, the minimum in solution shifts again to higher angles as is the case in air as shown in Figure 7a. The refractive index and the layer thickness can again be determined simultaneously for sufficiently thick layers only. For the LBL assembly, one finds a real part of 1.44 ± 0.01 and an imaginary part of 0.002 ± 0.001. The values are the same within experimental error for the zipper assembly, which suggests

dx.doi.org/10.1021/la2007815 |*Langmuir* 2011, 27, 7213–7221

that the optical properties of the thick films are similar for both assembly methods (Table 1). Given these values, the thickness of the layers can be determined by least-squares fit even for thin films reliably. The results are shown in Figure 7b, and one observes again that the thickness increases linearly with the number of deposited monolayers. For the LBL assemblies, one finds for one layer an increase in thickness of 3.66 ± 0.09 nm and for the zipper assemblies of 3.64 ± 0.08 nm. The increase in thickness with respect to the dry state and the corresponding swelling suggests the presence of defects in the wet state.

OPE-NDIs Data Analyzed Simultaneously. From the SPR measurement on dry and wet films, the volume fraction ϕ of water of the wet film can be obtained. From eq 5, one obtains from the respective thicknesses given in Table 1 a volume fraction of water of 0.47 ± 0.05 for the LBL film and 0.49 ± 0.05 for the zipper (Table 2). The other approach is to use the refractive indices and eq 6, and one obtains a volume fraction of water of 0.24 ± 0.06 for the LBL film and 0.25 ± 0.06 for the zipper. The discrepancy between these values could be related to film roughness and to the failure of the ideal mixing assumption. Since we are unable to decide which method gives more reliable results, the mean of these different estimates is taken find our best estimates of the volume fraction of water of 0.36 ± 0.08 for the LBL film and 0.37 ± 0.09 for the zipper. Here we arrive at the important result of this Article that the water content of the thicker LBL and zipper assemblies are the same within experimental error.

The density of the wet film ρ can be obtained from eq 2 by taking the thickness L of the wet film from SPR and the adsorbed mass Γ from QCM. One finds $\rho = 1.43 \pm 0.06$ g/cm^3 for the LBL assembly and 1.44 ± 0.06 g/cm^3 for the zipper. The density of the dry hybrid ρ_h can then be found from eq 4. With the value of the different water volume fractions ϕ determined above, one finds similar densities of the dry hybrid for the different assemblies (Table 2). Since one deals with the same hybrid, these values should be the same, which is almost the case within experimental error. Thus, the best estimate of the dry density of the hybrid can be obtained by taking the average of all the different values, and our best result is $\rho_h = 1.58 \pm 0.07$ g/cm^3.

Based on these quantities, one can find two additional physical-chemical parameters describing the adsorbed hybrids. The adsorbed mass of the dry film follows from eq 3 since the thickness in the dry film is known from SPR (Table 1). Different values are obtained based on the different water contents estimated, and the resulting values are summarized in Table 2. Since these estimates should be the same within experimental errors for the two different assemblies, taking the respective averages we find the best value $\Gamma_h = 0.31 \pm 0.02$ μg/cm^2 for the LBL assembly and basically the same value of 0.30 ± 0.02 μg/cm^2 for the zipper. With eq 7, one can also evaluate the refractive index increment, and the resulting values are summarized in Table 2 for the different assemblies and water contents. These are almost the same within experimental error as they should be, and our best estimate of the refractive index increment is 0.08 ± 0.01 mL/g.

Comparison between OPE-NDIs and POP-NDIs. The comparison of OPE-NDI photosystems (**2**-**3**-)$_n$ (Figure 1) with POP-NDI photosystems (**6**-**7**-)$_n$ (Figure 2) was of interest because their clear differences in activity suggested that the latter suffer from poor organization due to topological mismatch in the building blocks. Because of limited quantities of material available, studies with POP-NDIs had to be restricted to selected experiments only.

Since the normalized frequency shift in the QCM measurements was independent of the overtone number, the POP-NDI films are expected to be relatively rigid. The negative frequency shift increases again with increasing number of monolayers (Figure 8). This shift can be converted to the wet adsorbed mass with eq 1, and the corresponding wet mass is also shown in Figure 8. Fitting a straight line to these results, one finds an adsorbed mass of 0.50 ± 0.02 μg/cm^2 per layer for the LBL as

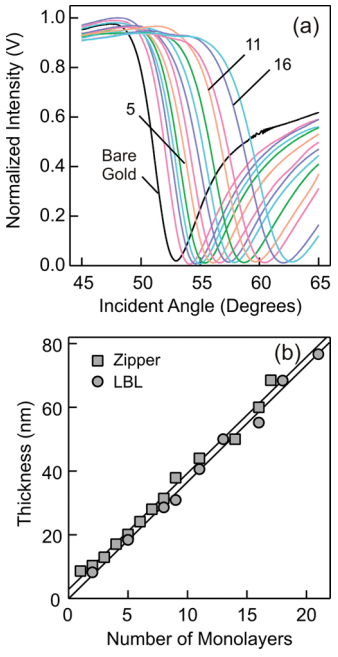

Figure 7. Analysis of wet OPE-NDI zipper film Au-**4**-(**2**−**3**-)$_n$ by SPR. (a) Series of SPR curves for different number of monolayers within the zipper assembly on the gold-coated SF10 prism in wet state. (b) Thickness calculated from SPR as a function of the number of monolayers deposited for OPE-NDI assemblies obtained by LBL and zipper techniques.

Table 2. Derived Quantities of OPE-NDI Films Obtained by Combining SPR and QCM Measurements

	LBL		zipper	
quantity	index[a]	thickness[b]	index[a]	thickness[b]
water volume fraction, ϕ	0.24 ± 0.06	0.47 ± 0.05	0.25 ± 0.06	0.49 ± 0.05
density dry layer, ρ_h (g/cm^3)	1.51 ± 0.11	1.63 ± 0.14	1.53 ± 0.11	1.67 ± 0.13
adsorbed dry mass, Γ_h (μg/cm^2)	0.29 ± 0.02	0.32 ± 0.03	0.28 ± 0.02	0.31 ± 0.02
refractive index increment, dn/dc (mL/g)	0.085 ± 0.009	0.078 ± 0.009	0.077 ± 0.009	0.071 ± 0.008

[a] Obtained by comparison of refractive indices of layers in dry and wet state. [b] Obtained by comparison layer thicknesses in dry and wet state.

dx.doi.org/10.1021/la2007815 |*Langmuir* 2011, 27, 7213–7221

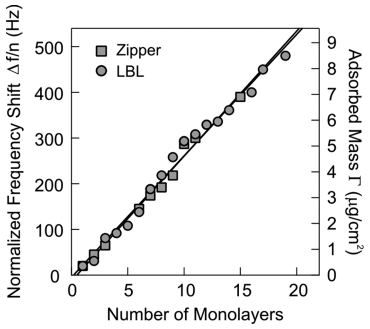

Figure 8. Analysis of POP-NDI LBL film Au-**1**-(**2**-**3**-)$_n$ by QCM. Negative frequency shift and wet mass as a function of the number of monolayers deposited for LBL and zipper technique.

Table 3. Properties of POP-NDI Films as Directly Obtained from QCM and SPR Measurements

technique	quantity	LBL	zipper
QCM	adsorbed wet mass, Γ (μg/cm^2)	0.50 ± 0.02	0.50 ± 0.02
SPR, dry film	real part refractive index, n_p	1.49 ± 0.02	1.50 ± 0.01
	imaginary part refractive index, k_p	0.031 ± 0.008	0.029 ± 0.005
	layer thickness, L_p (nm)	1.49 ± 0.03	1.45 ± 0.04

well as the zipper assemblies (Table 3). These results are in good agreement with previous QCM data on POP-NDI layers.[35]

Measurements on dry POP-NDI films were carried out with SPR. A typical sequence of reflectivity curves for different number of monolayers deposited is shown in Figure 9a. As with OPE-NDI architectures, the SPR minimum shifted to larger angles, indicating the increase in the thickness of the adsorbed film. The refractive index and layer thickness are determined independently for the thickest film consisting of about 20 layers. The real and imaginary parts of the refractive index are 1.49 ± 0.02 and 0.031 ± 0.008 for the LBL film, and one finds very similar numbers for the zipper assembly (Table 3). Once the refractive indices are known, one can determine the layer thickness from the SPR curves. The results are shown in Figure 9b. The thickness is a linear function of the number of monolayers deposited, and from the slope one finds the increase in thickness per layer. The found dry thickness per layer is 1.49 ± 0.03 nm for the LBL film and 1.45 ± 0.04 nm for the zipper assembly.

Based on these findings, the water content of the films can be estimated only by assuming the same dry density for the POP-NDI as for the OPE-NDI. This assumption is probably approximately correct. With eqs 2 and 4, one finds the water volume fraction ϕ of 0.52 ± 0.03 for the LBL and 0.54 ± 0.03 for the zipper assemblies. With this value at hand, the adsorbed mass of the dry film can be obtained, and its value is 0.23 ± 0.01 μg/cm^2 for both architectures.

These less complete studies with POP-NDI architectures already revealed two marked differences compared to OPE-NDI architectures. The first difference is that the monolayer thickness in the dry state is larger for the OPEs than for POPs, namely, about 1.9 and 1.5 nm, respectively. The second difference is the lower water content of the OPEs than for the POPs, namely, 36% and

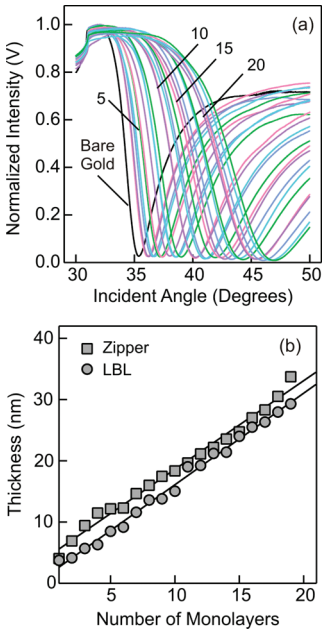

Figure 9. Analysis of POP-NDI LBL film Au-**1**-(**6**-**7**-)$_n$ by SPR. (a) Series of SPR curves for different number of monolayers within the LBL multilayer on gold-coated BK7 prism in dry state. (b) Thickness calculated from SPR as a function of the number of monolayers deposited for POP-NDI assemblies obtained by LBL and zipper techniques in dry state.

53%, respectively. The observed thickness for the OPE corresponds relatively well to one-half of the estimated largest hybrid length of about 3.5 nm as suggested by the zipper structure (Figure 1). The smaller thickness of the POP film could be related to a tilt within the layer (Figure 2). A tilt of the rigid-rod scaffold is expected to compensate for the too long repeat in the POP scaffold (~0.2 × 0.5 nm) compared to the repeat of an ideal NDI π-stack (0.35 nm).[35] This tilt of the POP scaffold in π-stack architecture has been proposed to disorganize zipper architectures[35] and yield helical photosystems rather than barrel-stave ion channels in lipid bilayers.[34] Contrary to the mismatched POP, the repeat in the OPE scaffold (~0.2 × 0.35 nm) perfectly matches the π-stack repeat and should thus afford "perfect" organization on surfaces. The poor responsiveness of POP-NDI (but not OPE-NDI) zippers to control experiments such as capping was in agreement with this interpretation.[35] The reduced thickness of POP-NDI architectures found in this study provides direct structural support for the expected tilting of POP scaffolds to compensate for topological mismatch. Moreover, the larger water content found for POP-NDI compared to OPE-NDI films is in excellent agreement for the disorganization caused by this mismatch.

It is instructive to compare the characteristics of the POP-NDI and well as OPE-NDI assemblies to the more common polyelectrolyte LBL assemblies. The internal structure of these layers was previously investigated by SPR, QCM, X-ray and neutron reflectivity.[29−31,35] From these studies, one knows that the thickness of a monolayer composed of either a cationic or anionic polyelectrolyte was around 2.5 nm at higher ionic strengths. The water content of such a multilayer is around 50−60%. Adsorbed polyelectrolyte monolayers tend to have even higher water content.[48,49] Their thickness is comparable, but this value strongly increases with the ionic strength. The individual polyelectrolyte monolayers are thus somewhat thicker than NDI

dx.doi.org/10.1021/la2007815 |*Langmuir* 2011, 27, 7213–7221

monolayers, and their water content is roughly comparable to the less organized POP-NDI multilayers investigated here. The unusually low water content found for the OPE-NDI architectures, however, was in excellent agreement with the expected "perfect" organization of these photosystems.

CONCLUSIONS

Multilayer zipper and LBL assemblies of artificial photosystems OPE-NDI and POP-NDI were studied with surface sensitive QCM and SPR techniques in dry and wet state. The obtained results provide a solid, quantitative basis for future studies on the topic. For the most interesting OPE-NDI zipper, this covers layer thickness (1.85 nm), refractive index (1.47), and density (1.58 g/cm^3) of the dry film and layer thickness (3.6 nm), refractive index (1.43), and water content (36%) of the wet film. The thickness of a monolayer in OPE-NDI zippers in the dry state corresponds to about one-half of the length of the OPE scaffold. This feature is in agreement with the proposed structure of the zipper. The thickness of the POP-NDI films (1.45 nm) in dry state is smaller than that for the OPE-NDI films (1.85 nm). This difference could be related to a tilt of the POP scaffolds within the adsorbed layer to compensate for the mismatch between the repeat in stacks and scaffolds. Even in solution, the OPE-NDI films are only weakly swollen with the solvent, which confirms their compact structure. The POP-NDI films swell in water much more substantially, supporting that their structure is much looser. These features are in line with the better performance of the OPE-NDI assemblies when compared to the POP-NDI films concerning the advantageous optoeletronic properties of OPEs compared to POPs to photocurrent generation (e.g., higher HOMO, better hole mobility, absorption of visible light).[35] These results are further consistent with the better responsiveness of OPE-NDI but not POP-NDI to functional controls that probe for supramolecular organization (e.g., assembly inhibition by capping). Note that a finite water in the wet state may be also caused by lateral imperfections of the films or surface inhomogeneities.

While the combination of SPR and QCM technique gives access to numerous characteristic properties of the layers, they are clearly insensitive to the orientation of the hybrids within the layer, which would distinguish the proposed zipper and LBL structures. The observed thicknesses agree well with the dimensions of the corresponding monolayers obtained from molecular models, but due to similar lengths and widths of the hybrids they are be expected to be the same. The layers are probably not crystalline, and will contain defects, which are likely to become increasingly important with increasing film thickness. Such structural parameters of these scaffolds could be assessed by off-specular reflection or X-rays or neutrons, but these are beyond the scope of this study.

As shown here, however, the topological and functional differences between POP-NDI and OPE-NDI photosystems are already reflected within the simple surface characteristics, such as thickness or water content. Due to similar lengths and widths of the building blocks, only minor differences between thickness or water content between the LBL and zipper assemblies were found. Only the slightly reduced layer thickness of dry OPE-NDI zippers (1.85 nm) compared to LBL assemblies (1.94 nm) can be seen as a support for a better, more compact organization of the former. The otherwise minor differences confirm that the photocurrents are determined by the local supramolecular organization rather than by the global structure of the films on larger scales. These findings are in excellent agreement with previous results on the activity of the photosystems.[35]

AUTHOR INFORMATION

Corresponding Author
*E-mail. michal.borkovec@unige.ch.

ACKNOWLEDGMENT

We thank D.-H. Tran, L. Maffiolo, S. Sakurai, and V. Ravikumar for contributions to synthesis and the University of Geneva, the ERC (Advanced Investigator, S.M.), the NCCR Chemical Biology (S.M.), and the Swiss National Science Foundation for financial support.

REFERENCES

(1) Bhosale, R.; Misek, J.; Sakai, N.; Matile, S. *Chem. Soc. Rev.* **2010**, *39*, 138–149.
(2) Wasielewski, M. R. *Acc. Chem. Res.* **2009**, *42*, 1910–1921.
(3) Yamamoto, Y.; Zhang, G. X.; Jin, W. S.; Fukushima, T.; Ishii, N.; Saeki, A.; Seki, S.; Tagawa, S.; Minari, T.; Tsukagoshi, K.; Aida, T. *Proc. Natl. Acad. Sci. U.S.A.* **2009**, *106*, 21051–21056.
(4) Hizume, Y.; Tashiro, K.; Charvet, R.; Yamamoto, Y.; Saeki, A.; Seki, S.; Aida, T. *J. Am. Chem. Soc.* **2010**, *132*, 6628–6629.
(5) Li, W. S.; Saeki, A.; Yamamoto, Y.; Fukushima, T.; Seki, S.; Ishii, N.; Kato, K.; Takata, M.; Aida, T. *Chem.—Asian J.* **2010**, *5*, 1566–1572.
(6) Wurthner, F.; Meerholz, K. *Chem.—Eur. J.* **2010**, *16*, 9366–9373.
(7) Huang, C. H.; McClenaghan, N. D.; Kuhn, A.; Bravic, G.; Bassani, D. M. *Tetrahedron* **2006**, *62*, 2050–2059.
(8) Crespo-Biel, O.; Ravoo, B. J.; Reinhoudt, D. N.; Huskens, J. *J. Mater. Chem.* **2006**, *16*, 3997–4021.
(9) Sugiyasu, K.; Kawano, S. I.; Fujita, N.; Shinkai, S. *Chem. Mater.* **2008**, *20*, 2863–2865.
(10) Balzani, V.; Venturi, M.; Credi, A. *Molecular Devices and Machines*; Wiley-VCH: Weinheim, 2003.
(11) Fukuzumi, S. *Bull. Chem. Soc. Jpn.* **2006**, *79*, 177–195.
(12) Martin, N.; Sanchez, L.; Herranz, M. A.; Illescas, B.; Guldi, D. M. *Acc. Chem. Res.* **2007**, *40*, 1015–1024.
(13) Yang, F.; Shtein, M.; Forrest, S. R. *Nat. Mater.* **2005**, *4*, 37–41.
(14) Roncali, J. *Acc. Chem. Res.* **2009**, *42*, 1719–1730.
(15) Kira, A.; Umeyama, T.; Matano, Y.; Yoshida, K.; Isoda, S.; Park, J. K.; Kim, D.; Imahori, H. *J. Am. Chem. Soc.* **2009**, *131*, 3198–3200.
(16) Edmondson, S.; Osborne, V. L.; Huck, W. T. S. *Chem. Soc. Rev.* **2004**, *33*, 14–22.
(17) Takada, T.; Lin, C.; Majima, T. *Angew. Chem., Int. Ed.* **2007**, *46*, 6681–6683.
(18) Kimura, S. *Org. Biomol. Chem.* **2008**, *6*, 1143–1148.
(19) Abdelrazzaq, F. B.; Kwong, R. C.; Thompson, M. E. *J. Am. Chem. Soc.* **2002**, *124*, 4796–4803.
(20) Martinson, A. B. F.; Massari, A. M.; Lee, S. J.; Gurney, R. W.; Splan, K. E.; Hupp, J. T.; Nguyen, S. T. *J. Electrochem. Soc.* **2006**, *153*, A527–A532.
(21) Morisue, M.; Yamatsu, S.; Haruta, N.; Kobuke, Y. *Chem.—Eur. J.* **2005**, *11*, 5563–5574.
(22) Koeppe, R.; Bossart, O.; Calzaferri, G.; Sariciftci, N. S. *Sol. Energy Mater. Sol. Cells* **2007**, *91*, 986–995.
(23) Wurthner, F.; Chen, Z. J.; Hoeben, F. J. M.; Osswald, P.; You, C. C.; Jonkheijm, P.; von Herrikhuyzen, J.; Schenning, A. P. H. J.; van der Schoot, P. P. A. M.; Meijer, E. W.; Beckers, E. H. A.; Meskers, S. C. J.; Janssen, R. A. J. *J. Am. Chem. Soc.* **2004**, *126*, 10611–10618.
(24) Bu, L. J.; Guo, X. Y.; Yu, B.; Qu, Y.; Xie, Z. Y.; Yan, D. H.; Geng, Y. H.; Wang, F. S. *J. Am. Chem. Soc.* **2009**, *131*, 13242–13243.
(25) Decher, G. *Science* **1997**, *277*, 1232–1237.

(26) Yu, G.; Gao, J.; Hummelen, J. C.; Wudl, F.; Heeger, A. J. *Science* **1995**, *270*, 1789–1791.
(27) Mwaura, J. K.; Pinto, M. R.; Witker, D.; Ananthakrishnan, N.; Schanze, K. S.; Reynolds, J. R. *Langmuir* **2005**, *21*, 10119–10126.
(28) Fushimi, T.; Oda, A.; Ohkita, H.; Ito, S. *Langmuir* **2005**, *21*, 1584–1589.
(29) Halthur, T. J.; Claesson, P. M.; Elofsson, U. M. *Langmuir* **2006**, *22*, 11065–11071.
(30) Losche, M.; Schmitt, J.; Decher, G.; Bouwman, W. G.; Kjaer, K. *Macromolecules* **1998**, *31*, 8893–8906.
(31) Steitz, R.; Leiner, V.; Siebrecht, R.; von Klitzing, R. *Colloids Surf., A* **2000**, *163*, 63–70.
(32) Zhao, L.; Ma, T.; Bai, H.; Lu, G. W.; Li, C.; Shi, G. Q. *Langmuir* **2008**, *24*, 4380–4387.
(33) Guldi, D. M. *J. Phys. Chem. B* **2005**, *109*, 11432–11441.
(34) Bhosale, S.; Sisson, A. L.; Talukdar, P.; Furstenberg, A.; Banerji, N.; Vauthey, E.; Bollot, G.; Mareda, J.; Roger, C.; Wurthner, F.; Sakai, N.; Matile, S. *Science* **2006**, *313*, 84–86.
(35) Bhosale, R.; Perez-Velasco, A.; Ravikumar, V.; Kishore, R. S. K.; Kel, O.; Gomez-Casado, A.; Jonkheijm, P.; Huskens, J.; Maroni, P.; Borkovec, M.; Sawada, T.; Vauthey, E.; Sakai, N.; Matile, S. *Angew. Chem., Int. Ed.* **2009**, *48*, 6461–6464.
(36) Sakai, N.; Sisson, A. L.; Burgi, T.; Matile, S. *J. Am. Chem. Soc.* **2007**, *129*, 15758–15759.
(37) Sisson, A. L.; Sakai, N.; Banerji, N.; Furstenberg, A.; Vauthey, E.; Matile, S. *Angew. Chem., Int. Ed.* **2008**, *47*, 3727–3729.
(38) Kishore, R. S. K.; Kel, O.; Banerji, N.; Emery, D.; Bollot, G.; Mareda, J.; Gomez-Casado, A.; Jonkheijm, P.; Huskens, J.; Maroni, P.; Borkovec, M.; Vauthey, E.; Sakai, N.; Matile, S. *J. Am. Chem. Soc.* **2009**, *131*, 11106–11116.
(39) Sakai, N.; Bhosale, R.; Emery, D.; Mareda, J.; Matile, S. *J. Am. Chem. Soc.* **2010**, *132*, 6923–6925.
(40) Bhosale, R.; Kishore, R. S. K.; Ravikumar, V.; Kel, O.; Vauthey, E.; Sakai, N.; Matile, S. *Chem. Sci.* **2010**, *1*, 357–368.
(41) Maity, S.; Bhosale, R.; Banerji, N.; Vauthey, E.; Sakai, N.; Matile, S. *Org. Biomol. Chem.* **2010**, *8*, 1052–1057.
(42) Edvardsson, M.; Rodahl, M.; Kasemo, B.; Hook, F. *Anal. Chem.* **2005**, *77*, 4918–4926.
(43) Hook, F.; Rodahl, M.; Kasemo, B.; Brzezinski, P. *Proc. Natl. Acad. Sci. U.S.A.* **1998**, *95*, 12271–12276.
(44) Beketov, G. V.; Shirshov, Y. M.; Shynkarenko, O. V.; Chegel, V. I. *Sens. Actuators, B* **1998**, *48*, 432–438.
(45) Rengevych, O. V.; Shirshov, Y. M.; Ushenin, Y. V.; Beketov, A. G. *Semicond. Phys., Quantum Electron. Optoelectron.* **1999**, *2*, 28–35.
(46) Wang, Y.; Pistora, J.; Lesnak, M.; Vlcek, J.; Stanek, F. *GeoScience Eng.* **2009**, *4*, 1802–5420.
(47) Johnson, P. B.; Christy, R. W. *Phys. Rev. B* **1974**, *9*, 5056–5070.
(48) Vaccaro, A.; Hierrezuelo, J.; Skarba, M.; Galletto, P.; Kleimann, J.; Borkovec, M. *Langmuir* **2009**, *25*, 4864–4867.
(49) Hierrezuelo, J.; Szilagyi, I.; Vaccaro, A.; Borkovec, M. *Macromolecules* **2010**, *43*, 9108–9116.